ARCHIVES OF ELECTRICAL ENGINEERING VOL. 72(1), pp. 239–252 (2023)

DOI 10.24425/aee.2023.143700

Strand wire winding method in a solenoidal coil with limited geometry for good impedance matching

VELI TAYFUN KILIC

Department of Electrical and Electronics Engineering
Abdullah Gul University
Kayseri, Turkiye
e-mail: tayfun.kilic@agu.edu.tr

(Received: 02.09.2022, revised: 21.11.2022)

Abstract: This paper reports a new strand wire winding method in a solenoidal coil with limited geometry that enables good impedance matching. In the proposed method strand wires are wound layer-by-layer on top of each other allowing one to set equivalent inductance and resistance of the coil to desired values while obtaining dense magnetic flux and high current carrying capacity. As a proof-of-concept demonstration, simple model setups were constructed with solenoidal coils composed of copper wire strands wound according to the proposed method, and a plastic pipe. The measurements were repeated with a metal shell placed inside the coil to model a complete heating system. System inductance and resistance were measured at two different frequencies. The results show that with the new winding method it is possible to increase a coil's turn number and the number of strand layers composed by the coil. Also, adding and removing strand layers in the proposed coil architectures enable inductance and resistance values to decrease and increase, respectively, in a controlled way. To understand changes of system parameters, simulations were also performed. The calculated inductance and resistance values in the simulations agree well with the measurement results and magnetic flux distribution created in the system demonstrates the changes.

Key words: solenoidal coil, strand wire, winding

1. Introduction

Near-field electromagnetics and induction systems are becoming more and more popular in today's world because of their advantages including high efficiency, safety, cleanliness, and good controllability [1, 2]. In induction systems, electromagnetic fields are produced by coils and these fields are coupled to and used by other system parts such as another coil or a metal plate [3].

There are various types of coils used in daily life for various purposes such as heating, melting, and wireless power transfer. Coil structures varies, depending on the application. For instance, pancake type coils are used in induction hobs because of their planar architecture [4–9]. Similarly, planar coils are chosen for wireless power transfer since they have a two-dimensional structure and can be mounted on a surface without causing too much altitude change [10–15]. On the other hand, solenoidal type coils are preferred to be used mostly for induction heating and melting applications [16–19] together with sensing operations [20–22]. Because of their three-dimensional structure, solenoidal coils enable the production of dense magnetic fields in their inner sides. Therefore, large induction currents can be produced on materials located inside solenoidal coils. In addition, because of their dense magnetic field, solenoidal-type coils are also used as inductors, especially in high-frequency circuits [23].

Although the density of the produced magnetic flux increases with a coil's turn number, there are trade-offs between a coil's turn number, wire radius, and wire's current carrying capacity. For instance, in a limited geometry, a coil's turn number cannot be increased forever by using a wire with a constant cross-section. To increase a coil's turn number, the winding wire diameter should be decreased. In other words, for a coil with a limited geometry, one way to increase the coil's turn number is to use thinner windings. However, as the diameter of the winding wire decreases, its current carrying capacity decreases too. In addition, coil impedance, i.e., its self-resistance and inductance, changes with its turn number together with the diameter and length of the winding wire. Coil impedance is important for good matching and efficient power transfer between the induction system and power supply circuitry. Therefore, in addition to geometrical limitations, one should also consider the impedance change of the coil while increasing the density of the produced magnetic flux inside the coil.

To overcome the aforementioned problems, in this study, we investigated a new strand wire winding method and obtained measurements with the manufactured prototype coil designs. In the designed coils, different from the conventional winding methods, wire strands are wound layer by layer on top of each other in rectangular column-shaped arrangement. The proposed method enables one to set inductance and resistance to desired values for good impedance matching without suffering too much from trade-offs between coil parameters, while allowing high-density magnetic flux in a solenoidal coil with a limited geometry. Also, to inspect the changes of the system, equivalent inductance and resistance values together with magnetic flux inside the coil three-dimensional (3D) electromagnetic (EM) simulations were conducted. The simulation results agree well with the measurement results.

2. Winding method and coil structure

In traditional coils, windings are usually made in the form of a solid filament or stranded litz wires, but because of the skin effect, especially at high frequencies, stranded wires are preferred [24–26]. In the coils made of litz wires, wire strands are first twisted and then these twisted strands are wound to form a coil winding. However, in these conventional litz wires, since wire strands with a determined number are twisted initially, there is no flexibility to change the number of strands and the diameter of the coil winding wire, which set the current carrying capacity of the wire.

To overcome the problem of the predetermined number of strand wires in a coil winding, the wire strands in the structure that we propose and investigated are wound layer by layer on top of each other. In this way, it is aimed to obtain a high turn number and a high number of strands, i.e., a high current carrying capacity, at the same time. The modelled strand wires having a rectangular column-shaped arrangement, are shown in Fig. 1.

Fig. 1. Wire strands with rectangular column-shaped arrangement

In regular systems during heating, process metal is placed inside a solenoidal coil. In our experiments, on the other hand, for easy production and for a firm coil structure, the coil wire is wound around a plastic pipe. Because plastic is a nonmagnetic material, its existence does not change the efficiency of induction power transfer that occurs wirelessly from coil wire windings to inside metal. Therefore, system electromagnetic parameters, such as equivalent impedance, do not change with plastic pipe's placement. In addition, because of the plastic material's properties of being thermally isolating and high temperature tolerant, we preferred to use it in our system. The used plastic pipe is commercially available and it consists of three layers. The inner and outer layers are made of polypropylene random (PPR) copolymer (Type3) material and between them there is a third layer comprising fiberglass [19].

In the manufacturing process with the proposed method, a single-strand wire is first wound over a plastic pipe continuously, such that the turn number (N) is high. After that, the second strand is wrapped over the first one with (trying to have) an equal turn number (N). Then the other strands, i.e., the third, the fourth, etc., are wound consecutively on top of each other. As a result, the strand layers in the manufactured coil are wound on top of each other, as shown in Fig. 2. In the figure, the strand wire's winding steps are illustrated too, seen from the side, on a constant plane passing through the center of the pipe. As seen, the windings on top of the pipe curl towards the inside and the windings on the bottom curl towards the outside. Although strand layers may also have different turn numbers, here we set their turn numbers to be equal. In this way, the magnetic flux contribution of each strand is aimed to be close. After wrapping all the layers, the start and end points of each layer (strand) are gathered and soldered. It is like we have coils wound on top of each other and connected in parallel.

In induction systems, for efficient heating, it is better the coil to completely cover the metal and in our case the plastic pipe. However, for easy production and more comfortable usage, it is possible to design a system in which the coil partly covers the metal. For instance, in a fluid heating system, the plastic pipe is clamped and covered at its ends while mounting between the pipes of the other system parts with a coil left open between them [19]. Therefore, in our produced system, we wound coil wire strands to cover not the whole but part of the plastic pipe. A very simple induction heating system, in which a pipe is partially encased by a coil, is presented in Fig. 3. In the figure, the pipe length and length of the pipe that is covered by the coil are labelled as L and l, respectively.

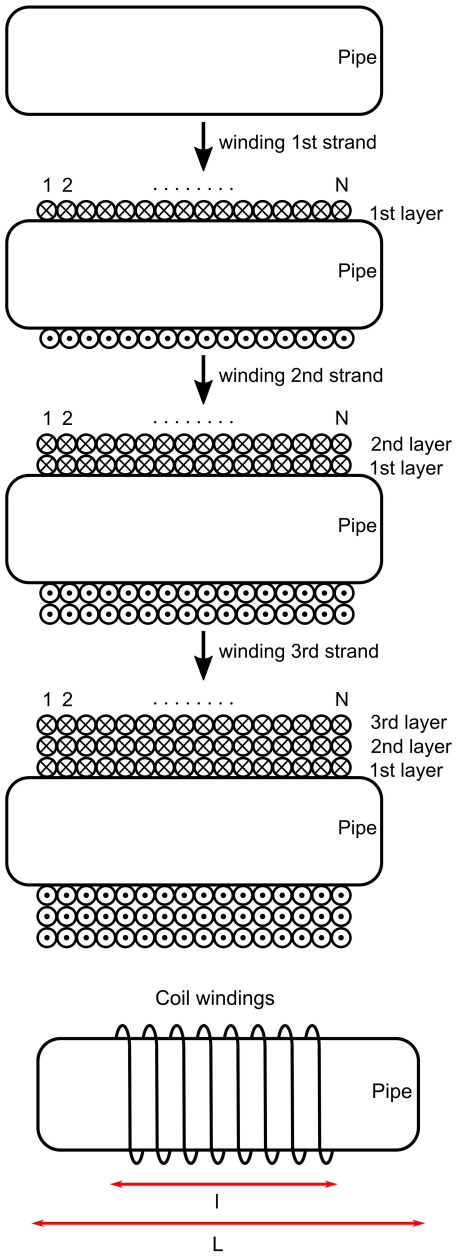

Fig. 2. Wire strands wound layer by layer on top of each other over a pipe. Here wire strands' winding steps are shown starting from bare pipe till the pipe covered by 3 layers. In the figure, $\times$ and $\cdots$ represent the inward and outward directions, respectively

Fig. 3. Very simple induction heating system in which part of a pipe is covered by coil windings

3. Measurement results and discussion

Measurements were conducted with the proposed structure (see Fig. 2). In the produced coils, the strand layers made of copper material with a circular cross-section having an outer diameter of 0.255 mm were wound to cover only 2 cm and 4 cm (l) of the pipe, which is 10 cm (L) long

in total (see Fig. 3). In addition, the plastic pipe has a wall thickness of 0.6 cm as well as inner and outer diameters of 2.9 cm and 4.1 cm, respectively. The equivalent resistance and inductance of the system were measured by means of an LCR meter through the end points of the coil. The measurements were obtained for different turn numbers and numbers of strand layers. In addition, these measurements were repeated at two different frequencies (20 kHz and 100 kHz), with and without a metal shell placed inside the plastic pipe. Specified frequencies were chosen because induction heating systems usually operate at a frequency between these two frequencies. Also, by repeating measurements with a metal shell it is aimed to model a complete induction heating system. The metal shell in the constructed system imitates metal objects that are placed inside solenoidal coils and heated up in induction systems. The measurement results are given in Table 1 and Table 2 for a coil covering length (l) of 2 cm and 4 cm, respectively.

Table 1. Measured equivalent resistance and inductance of the system with coil covering 2 cm of the pipe

Number of strand layers	**Turn numbers in layers (1st layer, 2nd layer, 3rd layer)**	**Frequency (kHz)**	**Metal shell existence**	**Resistance (Ω)**	**Inductance (μH)**
1	70	20	no	3.62	206.40
			yes	8.81	234.80
		100	no	3.79	206.26
			yes	15.83	208.98
2	70, 70	20	no	1.84	204.20
			yes	6.97	232.30
		100	no	2.14	204.00
			yes	14.05	206.70
3	70, 70, 70	20	no	1.27	203.60
			yes	6.40	231.70
		100	no	1.81	203.10
			yes	13.74	205.84

As seen, in the systems, where a metal shell is not placed inside the coil, the measured resistance value, i.e., coil's self-resistance, decreases almost linearly with the decrease in the coil covering length (l) and the turn number. For instance, in Table 1, the measured resistance values for turn numbers in layers equal to 70 are nearly half of the resistance values given in Table 2, for turn numbers of 135 in the layers. This is expected because the resistance of a coil winding is related to its length by (1).

$$R = \frac{(\rho \times l)}{A}, \tag{1}$$

where: R is the resistance (Ω), ρ is the resistivity of the winding strand material (Ω· cm), l is the length of the winding (cm) and A is the cross sectional area (cm^2) over which current flows. However, a linear behaviour is not obtained when a metal shell is placed inside the coil. Equivalent

Table 2. Measured equivalent resistance and inductance of the system with coil covering 4 cm of the pipe

Number of strand layers	**Turn numbers in layers (1st layer, 2nd layer, 3rd layer)**	**Frequency (kHz)**	**Metal shell existence**	**Resistance (Ω)**	**Inductance (μH)**
1	135	20	no	6.69	521.00
			yes	23.92	610.90
		100	no	7.05	521.10
			yes	45.82	528.50
2	135, 135	20	no	3.39	516.70
			yes	20.41	605.40
		100	no	3.99	516.80
			yes	42.28	524.20
3	135, 135, 135	20	no	2.33	511.20
			yes	19.14	598.60
		100	no	3.47	510.90
			yes	41.28	518.10

resistance decreases as the turn number decreases, but this decrease is faster than a linear decrease. This is because of the fact that part of the system's equivalent resistance arises due to additional power dissipated on the metal shell, which depends on the coupling between the coil windings and the metal shell.

In addition, the system's equivalent inductance decreases as the number of strand layers increases. This behaviour is observed in both system measurements with and without a metal shell, and interestingly, the obtained amount of decrease in both systems turned out to be very similar. Also, if one compares the tables, it is seen that as the turn numbers in layers decrease, the system's equivalent inductance decreases too. This decrease is faster than a linear decrease because the magnetic flux generated by a coil winding is proportional to the square of its turn number.

Moreover, it is seen in the tables that locating a metal shell inside the coil increases the equivalent resistance of the system. This increase is higher for measurements conducted at 100 kHz than for measurements taken at 20 kHz. The increase in the system's equivalent resistance with a metal shell placed is due to additional heat loss occurring on the metal shell as a result of finite conductivity of the metal and eddy currents produced on it. In addition, high enhancement in resistance for measurements conducted at 100 kHz is expected and can be explained by a decrease in the skin depth of the shell material at high frequencies. Similarly, the system's equivalent inductance increases with the placement of the metal shell inside the plastic pipe. This enhancement is higher at 20 kHz than at 100 kHz. The increase in the system's equivalent inductance when the shell is placed might not be expected at first look because eddy currents are induced over the metal shell, which is in opposite direction with that of the coil current and decreases magnetic flux produced by the coil.

The abovementioned observations and results can also be obtained in Fig. 4 and Fig. 5, where the equivalent resistance and inductance of the system with and without the metal shell at 20 kHz and 100 kHz frequencies are plotted for the cases of the coil covering 2 cm and 4 cm, respectively.

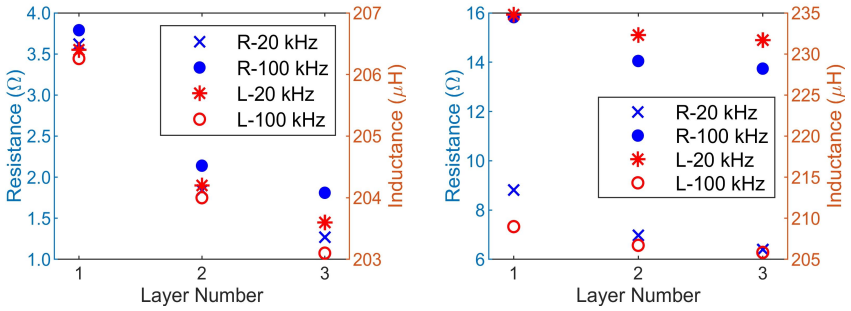

Fig. 4. Resistance and inductance of the system measured in experiments at 20 kHz and 100 kHz frequencies: (a) without the metal shell and (b) with the metal shell immersed into the coil having 70 turns in each layer and covering 2 cm of the pipe. In the legends of the figure, R and L indicate resistance and inductance, respectively

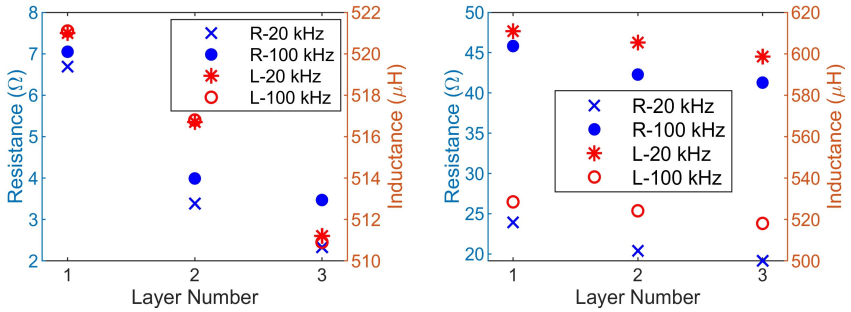

Fig. 5. Resistance and inductance of the system measured in experiments at 20 kHz and 100 kHz frequencies: (a) without the metal shell and (b) with the metal shell immersed into the coil having 135 turns in each layer and covering 4 cm of the pipe. In the legends of the figure, R and L indicate resistance and inductance, respectively

4. Simulations

To understand the system's equivalent inductance increase with the metal shell placement, 3D EM simulations were performed. In the simulations, coil structures, in which winding strands are wound layer by layer on top of each other, were drawn. In the modelled systems, the material of winding strands is chosen to be copper, and the radius of the strands that have a circular

cross-section is set to be equal to 0.127 mm. As in manufactured structures, coil wire strands in the modelled systems are wound around a plastic pipe. Geometry of the plastic pipe used in the simulations is set to be the same as that of the pipe employed in the measurements, such that the modelled pipe has a total length of 10 cm; and inner and outer diameters of 2.9 cm and 4.1 cm, respectively. In addition, the plastic pipe consists of three layers. The outer and inner layers are made of polypropylene random (PPR) copolymer (Type 3) films and the middle layer that is sandwiched between PPR copolymer films encompasses fiberglass. All three layers have the same wall thickness of 0.2 cm. Also, as in the measurements, the simulations of the system with the coil to cover 2 cm of the pipe with 70 turns in the layers were repeated with a metal shell placed inside the plastic pipe. The metal shell in the modelled systems is made of stainless steel with relative permittivity (ϵ_r) and relative permeability (μ_r) equal to 1 and 50, respectively, and an electrical conductivity (σ) of 1.39×10^6 S/m. The metal shell has a cylindrical geometry with a length of 100 mm, and inner and outer radii of 6.5 mm and 8.5 mm, respectively.

Exemplary systems with single- and 3-strand layers, modelled in the simulations, are shown in Figs. 6(a) and (b), respectively, seen from the side. Here, winding strands cover 2 cm of the pipe, and 70 turns exist in each winding layer. In the figure, for a clear illustration, close-ups of end points of the windings are presented in the insets. As seen in Fig. 6(b), for coils created with the proposed method and having multiple layers, winding strands are formed to be wound one above the other in column-shaped arrangement.

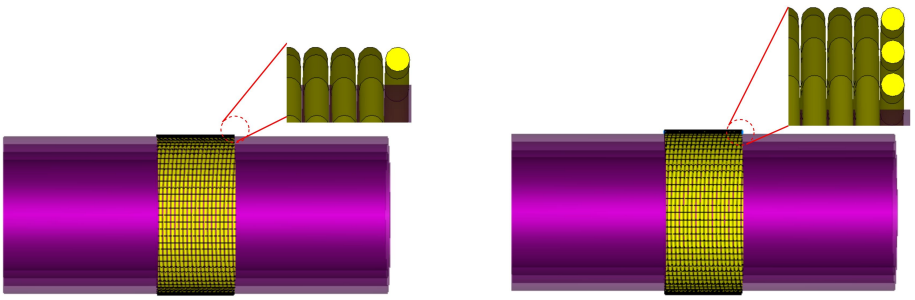

(a) (b)

Fig. 6. Side views of modeled coil structures in the simulation created with the proposed winding method having (a) single and (b) three layers. Here, winding strands occupy 2 cm on the pipe and 70 turns exist in each layer. Close-ups of end points of the windings are presented in the insets to clearly illustrate winding strands' being wrapped on top of each other in the introduced method

To make a fair comparison with the measurement results, the simulations were repeated at 20 kHz and 100 kHz frequencies for three different number of strand layers. In addition, the simulations were carried out for two different turn numbers in the layers equal to 70 and 135, which cover 2 cm and 4 cm of the pipe, respectively. The calculated equivalent resistance and inductance of the systems are given in Table 3 and Table 4. As different from Table 3, in Table 4, there is no column indicating metal shell existence inside the coil. The reason for this is the fact that the simulations of the system with the coil having high turn numbers in the winding strand

layers and the metal shell immersed in it were not performed as it required too much computer processor memory.

Table 3. Calculated equivalent resistance and inductance of the system with coil covering 2 cm of the pipe

Number of strand layers	**Turn numbers in layers (1st layer, 2nd layer, 3rd layer)**	**Frequency (kHz)**	**Metal shell existence**	**Resistance (Ω)**	**Inductance (μH)**
1	70	20	no	3.46	208.23
			yes	9.15	235.06
		100	no	3.72	208.13
			yes	18.49	209.45
2	70, 70	20	no	1.79	208.58
			yes	7.39	235.04
		100	no	2.29	206.47
			yes	17.61	207.34
3	70, 70, 70	20	no	1.27	209.16
			yes	6.97	233.47
		100	no	2.01	206.59
			yes	17.47	206.91

Table 4. Calculated equivalent resistance and inductance of the system with coil covering 4 cm of the pipe

Number of strand layers	**Turn numbers in layers (1st layer, 2nd layer, 3rd layer)**	**Frequency (kHz)**	**Resistance (Ω)**	**Inductance (μH)**
1	135	20	6.72	516.71
		100	7.25	516.49
2	135, 135	20	3.51	519.46
		100	4.55	515.50
3	135, 135, 135	20	2.70	521.22
		100	4.80	517.81

As seen, the inductance and resistance values calculated in the simulations and given in Table 3 and Table 4 are very similar to those measured and given in Table 1 and Table 2. Small differences between the calculated and measured resistance and inductance values are due to finite precisions of the simulations and measurements, as well as winding strands being not exactly the same as those modelled in the simulations.

As in the measurements, it is seen in Table 3 that both the resistance and inductance values calculated in the simulations increase with the placement of the metal shell. The resistance value increases are higher at 100 kHz than at 20 kHz, and it is explained by the decrease in the skin depth of the metal material as the frequency increases. The skin depth of the stainless steel used as the shell material in the modelled system is calculated to be 0.43 mm and 0.19 mm at 20 kHz and 100 kHz, respectively, by using (2)

$$\delta = \sqrt{\frac{1}{(\sigma \times \pi \times \mu_0 \times \mu_r \times f)}}, \tag{2}$$

where: δ is the skin depth, σ is the electrical conductivity of the material (1.39×10^6 S/m for the used stainless steel in the modelling), μ_0 is the free-space permeability ($4\pi \times 10^{-7}$ H/m), μ_r is the relative permeability of the material (50 for the used stainless steel in the modelling) and f is the operating frequency. On the other hand, the increase in the inductance value is an unexpected result at first glance. To understand and explain the enhancement of the system's equivalent inductance with a metal shell placed, the distribution of magnetic flux density over the system was investigated. Figure 7 shows the generated magnetic flux density distribution over the system, which consists of three-layer winding strands that cover 2 cm of the pipe and 70 turns exist in each winding layer with and without the metal shell when looking from the side on a constant plane passing through the centre of the pipe at 20 kHz.

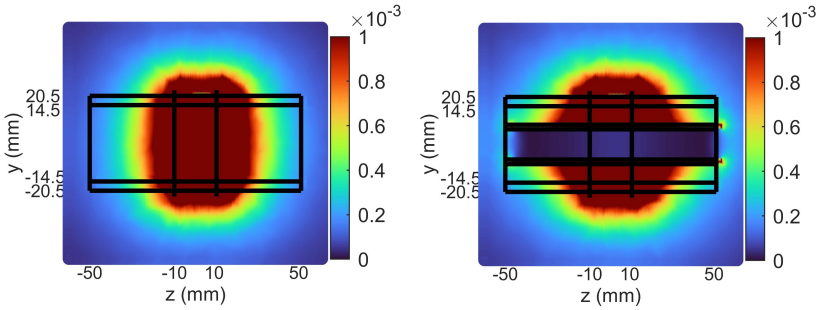

Fig. 7. Magnetic flux density distribution of the system: (a) without immersed metal shell and (b) with immersed metal shell, on constant x-plane that passes through the center of the pipe calculated in simulations at 20 kHz. Here, three layers of coil windings with 70 turns in each layer exist and the winding strands cover 2 cm on the pipe

In the figure, the end points of the plastic pipe are represented by horizontal black lines at $y = -20.5$ mm, –14.5 mm, 14.5 mm, 20.5 mm and vertical black lines at $z = -50$ mm, 50 mm. Also, lines at $y = -8.5$ mm, –6.5 mm, 6.5 mm and 8.5 mm are added in Fig. 7(b) to indicate the end points of the metal shell. Moreover, in both subfigures, the coil end points are pointed out with vertical lines at $z = -10$ mm and 10 mm. In Fig. 7(a) it is seen that the generated magnetic flux is focused on the inside of the plastic pipe, around the coil windings. This is expected because of the helical structure of the windings around the plastic pipe. On the other hand, in Fig. 7(b),

the magnetic flux density in the inner side of the metal shell is observed to be zero. This is due to the eddy currents induced on the metal shell. Since the current on the windings is in the opposite direction with the induced currents on the metal shell, the magnetic flux generated by the coil windings in the inner side of the metal shell is in the reverse direction to the magnetic flux produced by the induced eddy currents on the metal shell. In other words, in the inner side of the metal shell, the magnetic fluxes generated by the current flow on the coil windings and the induced eddy currents on the metal shell cancel each other. However, in Fig. 7(b), it is also seen that the magnetic flux density over the metal shell is high. This enhancement in the flux density continues along the shell. This is the reason why the equivalent system inductance value increases with the placement of the metal shell, despite zero flux density in the inner part of the metal shell. The high permeability and low magnetic reluctance of the metal shell cause the generated magnetic flux to concentrate over the metal shell, thus the equivalent magnetic permeability of the system and the equivalent system inductance value increase [27].

To clearly illustrate magnetic flux cancellation in the inner side of the metal shell and the magnetic flux concentrating over the shell magnetic flux density distribution in the system with and without the metal shell along the constant line that passes through the centre of the pipe, i.e., $z = 0$ mm, the line in Fig. 7 is plotted in Fig. 8. As seen, in the system with the metal shell, the generated magnetic flux is concentrated over the shell such that a peak density value of 0.066 V$\cdot$ s/m^2 is calculated on the outside wall of the shell, whereas the magnetic flux density in the inner side of the shell becomes 0. In the figure, y-axis intervals between ($-$8.5 mm, –6.5 mm) and (6.5 mm, 8.5 mm) at the top of the figure are marked with black colour to represent the metal shell thickness.

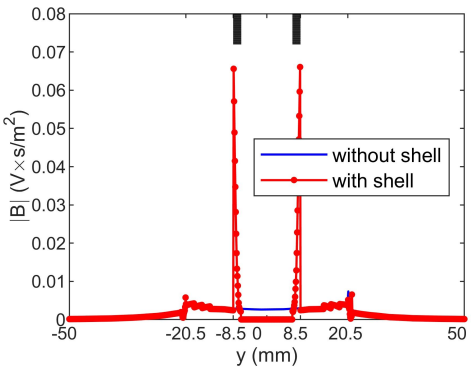

Fig. 8. Magnetic flux density distribution of the system with and without the metal shell along constant $z = 0$ mm line that passes through the center of the pipe in Fig. 7

5. Conclusion

This paper presents a new strand winding method in a solenoidal coil. In the proposed method, the strand layers that construct the coil wire are wound on top of each other forming a column-shaped arrangement. The inductance and resistance of coils having copper strand layer windings

were measured at different frequencies on manufactured prototypes. In the measurements, both the increase and decrease in inductance and resistance values were obtained while achieving very high turn number values and a high number of strand layers at the same time. The results show that the introduced method causes a linear relation between the self-resistance of a coil wound and the parameters, which are the length of the covered coil and the turn number. However, it was observed that the self-inductance of a coil wound with the presented method decreases as the number of strand layers increases. In addition, to model a complete heating system, the measurements were repeated with a metal shell placed inside the coil. Both the system equivalent inductance and resistance values are found to be increased when the metal shell was placed. Also, to understand the measurement results, 3D EM simulations were performed. The calculated inductance and resistance values match well with the measured ones. In addition, the magnetic flux density distribution of the systems calculated in the simulations verifies the inductance change of the system when the metal shell is placed.

The findings of this study are beneficial for the systems in which solenoidal coils with limited geometries are used in terms of proposing an alternative strand wire winding method that enables adjustment of the system's equivalent inductance and resistance values for good impedance matching together with a high turn number and high strand wire number allowing for a dense magnetic field and high current carrying capacity, respectively. A further extension of this work will include investigation of coils with the proposed winding method to be used in a specific application and their comparisons with commercially available coils.

Acknowledgements

The author would like to thank Emre Unal and Hilmi Volkan Demir for their help in the earlier coil manufacturing process and in the partial preparing of the manuscript.

References

[1] Acero J., Burdio J.M., Barragan L.A., Navarro D., Alonso R., Ramon J., Monterde F., Hernandez P., Llorente S., Garde I., *Domestic induction appliances*, IEEE Industry Applications Magazine, vol. 16, no. 2, pp. 39–47 (2010), DOI: 10.1109/MIAS.2009.935495.

[2] Lucia O., Acero J., Carretero C., Burdio J.M., *Induction heating appliances: toward more flexible cooking surfaces*, IEEE Industrial Electronics Magazine, vol. 7, no. 3, pp. 35–47 (2013), DOI: 10.1109/MIE.2013.2247795.

[3] Gao X., Li X., *Transmission characteristics of the mobile inductively coupled power transfer system for dual transmitters and pickups based on PSpice*, Archives of Electrical Engineering, vol. 69, no. 1, pp. 147–157 (2020), DOI: 10.24425/aee.2020.131764.

[4] Acero J., Alonso R., Burdio J.M., Barragan L.A., Llorente S., *Electromagnetic induction of planar windings with cylindrical symmetry between two half-spaces*, Journal of Applied Physics, vol. 103, no. 10, pp. 104905-1–104905-8 (2008), DOI: 10.1063/1.2903572.

[5] Kilic V.T., Unal E., Gonendik E., Yilmaz N., Demir H.V., *Strongly coupled outer squircle-inner circular coil architecture for enhanced induction over large areas*, IEEE Transactions on Industrial Electronics, vol. 63, no. 12, pp. 7478–7487 (2016), DOI: 10.1109/TIE.2016.2594228.

[6] Acero J., Carretero C., Lucia O., Alonso R., Burdio J.M., *Mutual impedance of small ring-type coils for multiwinding induction heating appliances*, IEEE Transactions on Power Electronics, vol. 28, no. 2, pp. 1025–1035 (2013), DOI: 10.1109/TPEL.2012.2205270.

[7] Kilic V.T., Unal E., Demir H.V., *Coupling and power transfer efficiency enhancement of modular and array of planar coils using in-plane ring-shaped inner ferrites for inductive heating applications*, Journal of Applied Physics, vol. 122, no. 1, pp. 014902-1–014902-7 (2017), DOI: 10.1063/1.4992119.

[8] Forest F., Faucher S., Gaspard J.Y., Montloup D., Huselstein J.J., Joubert C., *Frequency-synchronized resonant converters for the supply of multiwinding coils in induction cooking appliances*, IEEE Transactions on Industrial Electronics, vol. 54, no. 1, pp. 441–452 (2007), DOI: 10.1109/TIE.2006.888797.

[9] Kilic V.T., Unal E., Yilmaz N., Demir H.V., *All-surface induction heating with high efficiency and space invariance enabled by arraying squircle coils in square lattice*, IEEE Transactions on Consumer Electronics, vol. 64, no. 3, pp. 339–347 (2018), DOI: 10.1109/TCE.2018.2859627.

[10] Liu Y.R., Wang C., Xia D., Yue R., *Research on a novel hybrid shielding structure of magnetic coupler for inductive power transfer system*, Archives of Electrical Engineering, vol. 70, no. 1, pp. 129–143 (2021), DOI: 10.24425/aee.2021.136057.

[11] Kim D., Abu-Siada A., Sutinjo A.T., *Application of FRA to improve the design and maintenance of wireless power transfer systems*, IEEE Transactions on Instrumentation and Measurement, vol. 68, no. 11, pp. 4313–4325 (2019), DOI: 10.1109/TIM.2018.2889360.

[12] Saha C., Anya I., Alexandru C., Jinks R., *Wireless power transfer using relay resonators*, Applied Physics Letters, vol. 112, no. 26, pp. 263902-1–263902-5 (2018), DOI: 10.1063/1.5022032.

[13] Stoecklin S., Yousaf A., Volk T., Reindl L., *Efficient wireless powering of biomedical sensor systems for multichannel brain implants*, IEEE Transactions on Instrumentation and Measurement, vol. 65, no. 4, pp. 754–764 (2016), DOI: 10.1109/TIM.2015.2482278.

[14] Thuan N.V., Kang S.H., Choi J.H., Jung C.W., *Magnetic resonance wireless power transfer using three-coil system with single planar receiver for laptop applications*, IEEE Transactions on Consumer Electronics, vol. 61, no. 2, pp. 160–166 (2015), DOI: 10.1109/TCE.2015.7150569.

[15] Jolani F., Yu Y., Chen Z., *A planar magnetically coupled resonant wireless power transfer system using printed spiral coils*, IEEE Antennas and Wireless Propagation Letters, vol. 13, pp. 1648–1651 (2014), DOI: 10.1109/LAWP.2014.2349481.

[16] Terai H., Sadakata H., Omori H., Yamashita H., Nakaoka M., *High frequency soft switching inverter for fluid-heating appliance using induction eddy current-based involuted type heat exchanger*, 2002 IEEE 33rd Annual IEEE Power Electronics Specialists Conference Proceedings (Cat. No.02CH37289), Cairns, QLD, Australia, pp. 1874–1878 (2002).

[17] Gamage L., Ahmed T., Sugimura H., Chandhaket S., Nakaoka M., *Series load resonant phase shifted ZVS-PWM high-frequency inverter with a single auxiliary edge resonant AC load side snubber for induction heating super heated steamer*, The Fifth International Conference on Power Electronics and Drive Systems (PEDS 2003), Singapore, Singapore, pp. 30–37 (2003).

[18] Bui H.T., Hwang S.J., *Modeling a working coil coupled with magnetic flux concentrators for barrel induction heating in an injection molding machine*, International Journal of Heat and Mass Transfer, vol. 86, pp. 16–30 (2015), DOI: 10.1016/j.ijheatmasstransfer.2015.02.057.

[19] Kilic V.T., Unal E., Demir H.V., *High-efficiency flow-through induction heating*, IET Power Electronics, vol. 13, no. 10, pp. 2119–2126 (2020), DOI: 10.1049/iet-pel.2019.1609.

[20] Mandal N., Kumar B., Sarkar R., Bera S.C., *Design of a flow transmitter using an improved inductance bridge network and rotameter as sensor*, IEEE Transactions on Instrumentation and Measurement, vol. 63, no. 12, pp. 3127–3136 (2014), DOI: 10.1109/TIM.2014.2326770.

[21] Kim Y.S., Yu S.C., Lu H., Lee J.B., Lee H., *A class of micromachined magnetic resonator for high-frequency magnetic sensor applications*, Journal of Applied Physics, vol. 99, no. 8, pp. 08B309–08B309-3 (2006), DOI: 10.1063/1.2163840.

[22] Wei H.Y., Wilkinson A.J., *Design of a sensor coil and measurement electronics for magnetic induction tomography*, IEEE Transactions on Instrumentation and Measurement, vol. 60, no. 12, pp. 3853–3859 (2011), DOI: 10.1109/TIM.2011.2147590.

[23] Saini D.K., Ayachit A., Kazimierczuk M.K., *Design and characterisation of single-layer solenoid air-core inductors*, IET Circuits, Devices and Systems, vol. 13, no. 2, pp. 211–218 (2019), DOI: 10.1049/iet-cds.2018.5082.

[24] Wojda R.P., Kazimierczuk M.K., *Winding resistance and power loss of inductors with litz and solid-round wires*, IEEE Transactions on Industry Applications, vol. 54, no. 4, pp. 3548–3557 (2018), DOI: 10.1109/TIA.2018.2821647.

[25] Wojda R.P., Kazimierczuk M.K., *Winding resistance of litz-wire and multi-strand inductors*, IET Power Electronics, vol. 5, no. 2, pp. 257–268 (2012), DOI: 10.1049/iet-pel.2010.0359.

[26] Kazimierczuk M.K., *High-frequency magnetic components*, Wiley (2009).

[27] Snelling E.C., *Soft ferrites, properties and applications*, Iliffe Books (1969).